Energy Strategy Reviews 44 (2022) 100972

Contents lists available at ScienceDirect

Energy Strategy Reviews

journal homepage: www.elsevier.com/locate/esr

Making use of the complementarity of hydropower and variable renewable energy in Latin America: A probabilistic analysis

Miguel Gonzalez-Salazar [a], Witold Roger Poganietz [b,*]

[a] Berlin, Germany
[b] Institute for Technology Assessment and Systems Analysis (ITAS), Karlsruhe Institute of Technology (KIT), Kaiserstrasse 12, 76131, Karlsruhe, Germany

ARTICLE INFO

Keywords:
El niño southern oscillation
Hydropower
Photovoltaics
Wind power
Climate variability
Risk assessment

ABSTRACT

Latin America is one of the regions most vulnerable to the effects of climate variability on hydropower generation. Hydropower is the backbone of the Latin-American power system and a key technology for ensuring low-carbon power generation in the region. Despite its importance, our understanding of the impact and likelihood of seasonal variability and of long-term phenomena such as the El Niño Southern Oscillation (ENSO) on hydropower is limited. There is an essential need to understand how likely these effects are and to identify measures to counterbalance them. A combination of wind, solar, and hydropower offers the potential to mitigate the impact of climate variability on renewable power generation and thus improve its reliability. Here we present a modeling framework to quantify the potential benefits of such combination. The modeling framework relies on a meteorological reanalysis dataset, large-scale renewable power generation models, and statistic models. We consider the countries with the largest hydropower capacity in the region, namely Argentina, Brazil, Colombia, Mexico, and Venezuela. We examine whether the probability of a production deficit is reduced when all renewable resources are combined compared to a scenario based solely on hydropower, especially during droughts. The approach presented allows for the first time an in-depth analysis of the benefits of a combined wind, solar, and hydropower-based power generation under different geographical conditions in altered ENSO phases.

Our results suggest that—depending on the country and the percentile—the hydropower generated during drought ENSO phases could be up to 50% lower than that during neutral phases. The countries most affected are Colombia and Venezuela, while the reduction is somewhat less severe in Argentina, Brazil, and Mexico. Combining hydropower with variable renewable energy (VRE) offers the potential to reduce the risk of a power deficit during the 10th percentile of the driest months of the year, both in drought and neutral phases. Argentina is the country with the most effective combination of resources to mitigate a power deficit, as each MW of installed VRE generates 0.218 GWh of additional power. It is followed by Brazil and Mexico with 0.185 GWh per MW of VRE and by Venezuela and Colombia with 0.128–0.098 GWh/MW of VRE, respectively. These results can contribute to informing future decisions on capacity planning and regional transmission grids.

1. Introduction

The backbone of the renewable electricity system in Latin America is hydropower, which is vulnerable to seasonal variability and to the long-term phenomenon El Niño Southern Oscillation (ENSO). ENSO is a large-scale ocean-atmosphere climate interaction that manifests as a fluctuation in sea-surface temperature (El Niño) and in the air pressure of the overlying atmosphere (Southern Oscillation) across the Pacific Ocean [1]. ENSO is characterized by two active alternating and irregular phases and an inactive or neutral one. Each of the active phases, which are distinguished in a warming (El Niño) and a cooling (La Niña) phase, lasts several months, influencing adversely rainfall patterns, droughts, floods [1], hydropower generation [2], and consequently commodity prices [3]. ENSO has been found to strongly affect renewable power generation in nearly all the states bordering the Pacific Ocean [4–7].

To reduce the vulnerability to seasonal variability and ENSO and improve the reliability of electricity provision, Latin America is currently experiencing a steady increase in gas-based electricity generation along with rapid growth in variable renewable energy (VRE), i.e., solar and wind power [8–11]. The increase in gas power plants

* Corresponding author.
E-mail addresses: gnzmln@unife.it (M. Gonzalez-Salazar), witold-roger.poganietz@kit.edu (W. Roger Poganietz).

https://doi.org/10.1016/j.esr.2022.100972
Received 25 January 2022; Received in revised form 8 September 2022; Accepted 2 October 2022
Available online 6 October 2022

counteracts the global and regional aims of decreasing the carbon footprint of the energy system [8,12]. Renewable energy is today one of the most effective measures to mitigate climate change [13–16]. Exploiting complementarities between hydropower and other renewables could be seen as an alternative for enhancing the reliability of electricity generation while mitigating the impact of seasonal variability and ENSO on hydropower. In this study, complementarity refers to the extent to which production shortfalls of one energy technology, i.e., hydropower, can be compensated by other energy technologies, i.e., wind and solar photovoltaic (PV) power [17].

A dedicated literature review is performed and details are shown in Appendix A. Prior art has investigated the complementarity between hydropower and other renewable energy sources, concentrating mostly on wind and PV power [17]. From the point of view of the geographic scale, the majority of the studies focus on sub-national or national scales, while a few studies have addressed complementarity at a multi-national or continental scale. The majority of studies focus on finding the best design of the power system and its operation schedule on short temporal scales, ranging from minutes to days. However, little research (e.g. Refs. [5,18]) has been devoted to exploit complementarity between renewables to mitigate long-term (interannual, multiannual scales) phenomena like ENSO. Regarding the method, prior studies have used deterministic approaches more often than probabilistic (stochastic) approaches. Whereas the former approaches are based on a rigid set of assumptions regarding the objective function and underlying market conditions, the latter allow for different operational objectives and market conditions. Although these studies consider the risk profile of renewable energy sources, they seldom calculate explicitly the impact of the complementarities on the risk profile of hydropower.

Various studies have used a deterministic approach and focused on Latin America. They have explored the complementarity between two or three pairs of renewable resources at country [19–28] and regional levels [8,16,29], as well as the influence of climate change on it [16]. These studies analyzed spatio/temporal complementarity with data obtained either from measured data in existing units or by simulating the performance of potential units using meteorological data dating back to 1975 at most. In a recent investigation, the authors of this study show that exploiting the complementarity between different renewable energy resources has the potential to cost-effectively compensate for the fluctuations in hydropower and reduce the variability of power generation caused by ENSO in various countries in Latin America [30].

Studies focusing on probabilistic approaches for evaluating the complementarity between resources are scarcer. Li et al. [31] have used stochastic dynamic programming to show that the large-scale hydro-PV hybrid power plant Longyangxia in Qinghai province, China, could increase the total generation and total guaranteed rate by up to 6.7% and 22.9%, respectively, compared to a conventional hydropower plant. A hybrid power plant could also help to shave short-term demand peaks [32]. Huang et al. [33] have performed a probabilistic optimization to reduce the output shortage when combining hydro, wind and PV in the Guandi power plant on China's Yalong River. Similarly, Zhang et al. [34] have performed a multistage stochastic optimization to improve the dispatch of a hydro-wind system in southwest China. Schmidt et al. [35] assessed for the Brazilian electricity system how high the long-term shares of renewable electricity production can be maintained, while reducing hydrological risks in case of an increasing demand for electricity. Using an optimization model, their findings indicate that adding solar PV and wind to the current energy system would diminish the necessity to run thermal power as a backup and the risk of loss of load. The total variability of renewable supply decreases significantly in comparison to a scenario that adds only hydropower to the system. This finding has been confirmed by Luz and Moura [36]. As a consequence, the planning of future power systems should recognize these complementarities at an early stage, avoiding nonideal investments and intending to increase the reliability of the grid [26]. It should be noted that adverse effects on the long-term availability of hydropower could happen if the flexibility of hydropower is overstretched [37]. Denault et al. [38] use as a measure of risk the probability of a production deficit, comparable to approaches used in financial risk management [38]. Taking the province of Quebec, Canada, as a reference their results indicate that any wind power share in the electricity mix below 30% reduces the risk of a production deficit compared to an all-hydropower system by lowering the dependence on water inflows and attenuating the impact of droughts.

Summing up, there is a lack of studies evaluating from a probabilistic perspective the combination of hydropower with VRE to reduce the vulnerability of the power system with respect to droughts and ENSO in a multi-national context. This paper aims at filling this gap. The overarching aim of this paper is to analyze the impact that connecting existing hydropower with complementary VRE could have on the reliability of the power generation in Latin America, particularly under the conditions of the long-term phenomena ENSO. In contrast to prior studies, we don't analyze any kind of wind and solar resources to supplement existing hydropower. Instead, we consider only VRE resources that offer at least a complementarity of −50% with existing hydropower (i.e., a Spearman correlation coefficient of −0.5). Connections with less complementarity are excluded in the study. To evaluate this complementarity, we simulate time series of solar, wind and hydropower for the entire twentieth century for the countries with the largest hydropower capacities in Latin America (i.e., Brazil, Venezuela, Argentina, Mexico, and Colombia). Then, we create multiple portfolios with varying degrees of penetration of VRE for each country. For each scenario, we build probability density functions, i.e., risk profiles for solar, wind and hydropower. These risk profiles are significantly affected by seasonal variability and the long-term phenomena ENSO. We investigate the impact that the different portfolios could have on reducing the risk of a possible power deficit, which is defined here as the power shortage that occurs once every decade, i.e., the 10th percentile of the driest months of the year for each country. Finally, we identify strategies to mitigate a situation of a possible power deficit caused by seasonal variability or ENSO drought.

The paper is structured as follows. Section 2 describes the method used in this investigation. Section 3 presents the process of identifying the appropriate combinations of wind, solar, and hydropower resources, including an analysis of their dependencies. Section 4 is devoted to the probabilistic analysis of the different energy resources, as well as the impact of combining hydropower and VRE to mitigate power deficits. Concluding remarks are shown in Section 5.

2. Method

The aim of this paper is to analyze the impact that combining existing hydropower with greenfield and complementary VRE could have on the reliability of the combined power generation in Latin America, particularly under the conditions of the long-term phenomena ENSO. Wind and solar are thus envisaged as diversification strategies to reduce the risk of a production deficit of the power generation system (hydropower + VRE). Because the duration of a drought can range from months to years, we have focused our analysis on these temporal scales. Thus, we purposely exclude short-term operational constraints. While short-term effects typically cancel out in the long-run, as pointed out in previous studies [39,40], they exert a strong impact on the operability of wind, solar, and hydropower in day-ahead or intraday electricity markets, which are not analyzed here. This implies a limitation of the study, which does not affect the validity of the findings on a long-term temporal scale. To estimate the uncertainty in power generation, we present an analysis framework that relies on a meteorological reanalysis dataset, three large-scale renewable power generation models, and statistical models.

2.1. Framework

The proposed framework is explained in Fig. 1. In Step 1, we identify the relevant combination of hydropower with VRE. To achieve this, we have generated a time series of monthly power generation for the entire twentieth century, combining a high-fidelity hydropower dam model and two large-scale land-based wind and solar power generation models with a meteorological reanalysis dataset (the WATCH forcing data). These models are described in Section 2.2 and are also detailed in Ref. [30]. A deeper assessment, was conducted on the countries with the largest hydropower capacities in Latin America, i.e., Brazil, Venezuela, Argentina, Mexico, and Colombia. For hydropower, all the dams available in these countries were selected from a dataset created by Ng et al. in Ref. [2].

There are various measures to quantify the dependence between two variables. The most common measures for evaluating the complementarity between renewables include the Pearson correlation coefficient, the Kendall correlation coefficient, and the Spearman correlation coefficient [17]. The most common method is the Pearson correlation coefficient, which evaluates the linear correlation between two sets of data. It is the ratio between the covariance of two variables and the product of their standard deviations. A key advantage of the Pearson correlation coefficient is its simplicity and intuitive interpretation. However, its main disadvantage is that it can only evaluate linear relationships between two variables, i.e., it cannot effectively evaluate non-linear relationships [17]. Kendall and Spearman correlation coefficients aim at addressing this limitation. Rather than measuring the linear correlation between variables, these two coefficients evaluate the monotonic relationship, i.e., the degree that two variables move in the same direction, but not necessarily at a constant pace. While both coefficients have been used to a similar extent in previous studies of complementarity, neither is clearly superior to the other [17]. Hence, we have selected the Spearman coefficient. The Spearman correlation coefficient is a measure of the dependence between the rankings of two variables (x, y):

$$S_{x \leftrightarrow y} = \frac{\mathrm{cov}(r.x, r.y)}{\sigma_{r.x} \bullet \sigma_{r.y}} \tag{1}$$

where $S_{x \leftrightarrow y}$ is the Spearman correlation coefficient between x and y, r. x and r. y are the rankings of variables x and y, $\sigma_{r.x}$ and $\sigma_{r.y}$ are the standard deviations of the rank variables, and $\mathrm{cov}(r.x, r.y)$ is the covariance of the rank variables. The lower the Spearman correlation coefficient, the better the complementarity between two resources, with -1 indicating optimal complementarity. We selected wind and solar resources offering at least a Spearman correlation coefficient of -0.5 with hydropower at a country level [30].

For wind and solar power, only those resources with a high level of complementarity with hydropower at a country level were taken into account. For each of these resources, the average power generation throughout the entire twentieth century is estimated, and then aggregated countrywise on a monthly and annual basis. To analyze the data, the monthly power generation is categorized countrywise according to the ENSO intensity and to the ENSO phase that most strongly affect hydropower. To classify the data according to the ENSO intensity, the Multivariate ENSO Index (MEI) is employed. MEI characterizes the intensity of ENSO events by combining six meteorological and oceanographic parameters [41]. Months throughout the twentieth century are grouped into three categories: (*i*) months within the 10th percentile of MEI, describing La Niña events, (*ii*) months between the 10th-90th percentiles, describing neutral phases, and (*iii*) months above the 90th percentile, describing El Niño events.

In Step 2, we analyze the impact of complementarity on power generation, focusing on seasonal and ENSO droughts. To accomplish this, we simulated different portfolios of aggregated wind, solar, and hydropower capacity in a process consisting of three sub steps. First, we created portfolios with different combinations of hydropower and VRE (i.e., wind and solar PV). Next, statistical models were created and calibrated with the time series for wind, solar, and hydropower generated in step 1. Since we are concerned with power deficits caused by droughts, we selected the month of the year with the lowest hydropower generation for each country. Based on this selection, we estimated the probability of generating power for these months across the different scenarios. For accomplishing this, we use probability density functions (PDFs) and cumulative distribution functions (CDFs) for the observed time series. We focused on the power deficit that occurs once every decade, i.e., the 10th percentile of the probability functions of the driest month of the year. This approach follows the procedure described in Ref. [38]. Finally, we compare the risk measures across portfolios for all the countries.

Finally, in step 3, we identify strategies to mitigate a situation of a possible power deficit caused by seasonal variability or ENSO drought. In particular, we evaluate how much wind and solar power are needed to counteract the power deficit that occurs once every decade, especially during ENSO drought phases.

2.2. Modeling wind, solar and hydropower

The modeling approach used for evaluating the power generation

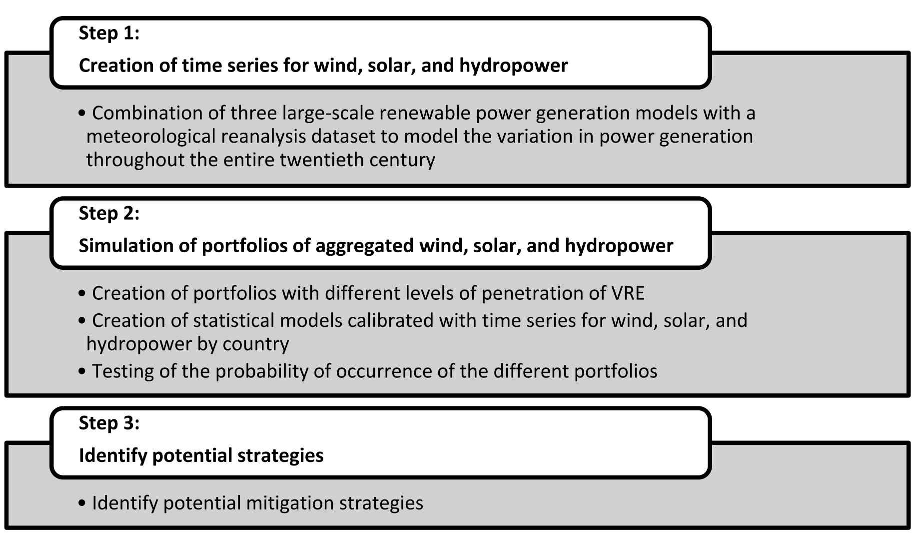

Fig. 1. Proposed framework.

from hydro-, solar- and wind-power throughout the 20th century is described in the following sections and illustrated in Fig. 2. We primarily use the meteorological reanalysis dataset WATCH forcing data (WFD) to extract key variables such as wind speed, air temperatures, and downward shortwave radiation flux with a 0.5 x 0.5 geographical resolution and 3- or 6-hourly time resolution throughout the 20th century. We then evaluate the area suitable for installing wind and solar plants. We use the Terra and Aqua combined Moderate Resolution Imaging Spectroradiometer (MODIS) Land Cover Climate Modeling Grid (CMG) (MCD12C1) and availability factors found in literature. The core of the modeling approach is the combination of a high-fidelity hydropower dam model (for evaluating existing hydropower plants) and two large-scale land-based wind- and solar-power generation models (for evaluating greenfield VRE plants). Subsequently, we employ a statistical algorithm to find the complementarity between pairs of hydro-solar, hydro-wind and wind-solar sites based on their power generation throughout the entire 20th century. We down select sites that offer a minimum of −50% complementarity (using the Spearman correlation coefficient) for further analysis. Finally, for the selected sites, we perform the risk evaluation described above.

2.2.1. Estimation of available land for deploying wind and solar

We assessed the area available for installing wind turbines and solar PV at a country level after considering environmental conditions, availability, and economic constraints. We use the Terra and Aqua combined Moderate Resolution Imaging Spectroradiometer (MODIS) Land Cover Climate Modeling Grid (CMG) (MCD12C1) Version 6 [42] to extract the spatial distribution of the different types of land cover for the year 2018. This data product provides information at yearly intervals at 0.05-degree spatial resolution for the entire globe from 2001 to 2018. Eq. (2) is used to estimate the area suitable for installing wind turbines and solar PV (A_S):

$$A_S = A_{LC} - A_{UL} - A_{PL} \tag{2}$$

where from the total land cover (A_{LC}) we exclude land unsuitable for installing renewable energy technologies (A_{UL}) and protected land (A_{PL}). Unsuitable land includes areas classified as forest, closed and open shrubland, wetland, areas with permanent snow or ice, areas covered by water and urban areas. Then, we exclude protected areas using the protected area coverage data available at the Digital Observatory for Protected Areas [43,44], which has a resolution of approximately 10 km. We use netCDF4 and NumPy libraries in Python to parse the data and aggregate it at 0.5-degree spatial resolution for year 2018. The resulting area suitable to install wind turbines and solar PV is shown per cell of 0.5 × 0.5° in Fig. 11 (left) in Appendix B.

While this is the area suitable for installing these technologies, not all of it is actually available as it might be allocated for other uses. To assess the area actually available for deploying wind and solar installations, we used availability factors that describe the share of land which can be used for installing RES technologies, due to land competition, following the approach used in prior research [45,46]. The idea behind this approach, is that only a small fraction of the suitable area in a given grid cell is likely to be available to deploy wind or solar. Eq. (3) estimates the area available for installing wind turbines and solar PV (A_I):

$$A_I = k_a \bullet (A_S - A_{TU} - A_{Add}) \tag{3}$$

where k_a is the availability factor for wind and solar disaggregated by

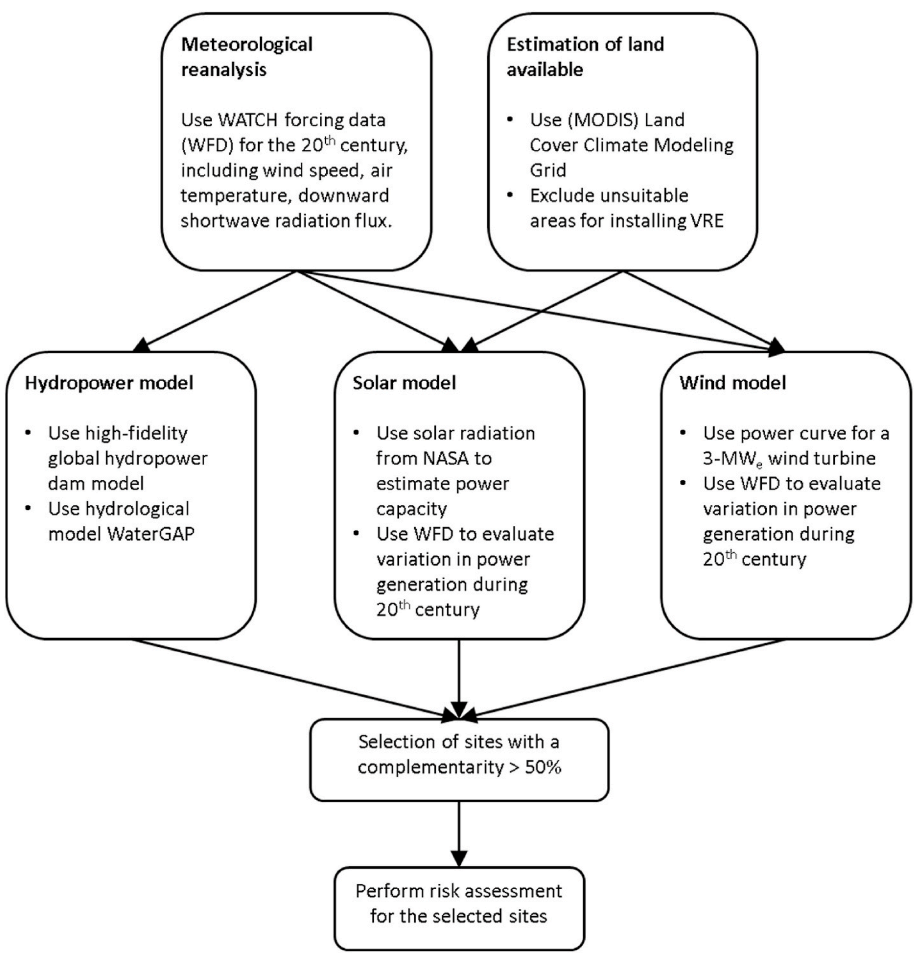

Fig. 2. Modeling approach.

the type of land cover derived from the literature [46,47], see details in Ref. [30]; A_{TU} is the area technically uneconomical due to a poor energy potential, more concretely we exclude areas with a capacity factor of wind-power below 20% [45] and with a solar irradiance below 950 kWh/m^2 [46]. Finally, we have an additional environmental restriction (A_{Add}), in which neither wind nor solar is likely to be deployed if the protected area coverage within the cell (0.5 × 0.5°) is higher than 15%. The resulting areas available for installing solar PV and wind power per cell of 0.5° (not continuous variables) are shown in Fig. 11 (middle and right) in Appendix B.

2.2.2. Hydropower model

A high-fidelity global hydropower dam model developed by Ng et al. [2,48] is used, which helps to replicate about 65% of the existing installed capacity in the region, i.e., 150 existing hydropower dams across Latin America. This model compiles data on the design specification of 1593 existing hydropower dams from the GRanD database [49], and on installed power capacities from the ICOLD [50] and Global Energy Observatory [51] databases. The model includes run-of-river dams, but excludes pump-storage reservoirs. For each dam a monthly time series throughout the entire twentieth century is developed using the WFD model output [52]. The runoff data are generated by forcing a global hydrological model (WaterGAP [53]) that computes accumulated runoff using the DDM30 river network [54]. The hydropower model simulates the decision making of the hydropower dam operators using a periodic Markov chain algorithm for each dam. The model is implemented using the R package *reservoir* [55]. As historical data on actual operation of individual dams are unavailable, the model is validated against coarser data on a national basis and only for the years 1980–2000. The validation resulted in strong fits for hydropower generation in most countries (Pearson coefficients between 70 and 95%) but had limited ability to predict capacity factors.

2.2.3. Wind model

Following a methodology proposed by Lu et al. [45], a land-based wind model is developed using Python (NumPy, netCDF4 and Shapely libraries). Wind offshore has been excluded, as its cost-effectiveness in the short to medium term in the region is uncertain and its deployment is expected to remain marginal [56].

The wind power output is calculated based on wind conditions for each grid cell (0.5 × 0.5°) and a power curve of a real turbine. Suitability factors are applied for deploying wind turbines based on the land cover, and excluded forests, environmentally sensitive areas, and water bodies. For assessing the wind conditions at each grid cell (6500 in total), three variables with 6-hourly time steps are extracted from the WFD dataset [52,57], namely the surface pressure (P_{Surf}), the air temperature at 2 m (T_{air}), and the wind speed at 10 m (WS_{10}). Then, the power curve is employed to quantify the electrical power output as a function of wind speed and air density. Hereby, the Vestas V90-3.0-MW is selected, a pitch regulated upwind wind turbine with three-blade rotor and a rotor height of 90 m [58]. Since the wind speed from WFD is available at 10 m, it is estimated at 90 m (WS_{90}) using a power law relationship that is independent of roughness lengths [59]:

$$WS_{90} = WS_{10} \bullet (90/10)^{0.143} \tag{4}$$

Then, the air density (ρ) at the rotor height is estimated as:

$$\rho = P_{Surf} \Big/ (R \bullet T_{air}) \tag{5}$$

where R is the gas constant (287.04 J/kg-K). With the wind speed and the air density it is possible to calculate the power generation at 6-hourly time steps ($PG_{W,y}$), using the power curve in Fig. 12 in Appendix B. Then, for each grid cell the power generated is aggregated to monthly and annual bases and the corresponding capacity factor is calculated. Finally, the technical annual wind potential ($G_{W,y}$) and power capacity (P_W) for each grid cell are calculated as:

$$G_{W,y} = A_{I-W} \bullet PG_{W,y} / N_W \tag{6}$$

$$P_W = A_{I-W} \bullet P_{W-UNIT} / N_W \tag{7}$$

where A_W is the area available for installing wind turbines in each grid cell (km^2), $PG_{W,y}$ is the annual power generated by an individual wind turbine (GWh/year), P_{W-UNIT} is the power capacity for a single wind turbine (3 MW), N_W is the occupation area per turbine (km^2/unit) and subscript *y* means annual. The monthly wind-power generation is calculated in the same manner. The area available for installing wind turbines ($A_{I\text{-}W}$) is assessed after considering various constraints, as explained above. Firstly, forests, environmentally sensitive areas, and water bodies are excluded. Secondly, availability factors are applied based on the land cover. Thirdly, areas with a wind capacity factor below 20% are excluded as they appear uneconomical. The occupation area per turbine is 0.28 km^2/unit, following Lu et al. [45].

2.2.4. Solar model

A land-based solar PV model is created following a methodology proposed by Jerez et al. [14]. The power generation from PV utility-scale centralized systems (i.e., PV systems mounted on land and not on building roofs) is estimated as a function of two factors: the performance factor (F_{PV}) and the power capacity (P_{PV}). The performance factor is a dimensionless variable quantifying the deviation of the performance of PV at actual ambient conditions with respect to their nominal power capacity. The power generation results from multiplying F_{PV} and P_{PV}. The performance factor can be described as:

$$F_{PV} = \left(\frac{SWD}{SWD_{TC}}\right) \bullet [1 + \gamma(T_{cell} - T_{TC})] \tag{8}$$

where SWD is the downward shortwave radiation flux (wavelength interval 0.2–4 μm), SWD_{TC} refers to the radiation flux standard test conditions (1000 W m^{-2}), T_{cell} is the PV cell temperature, T_{TC} is the temperature at standard conditions and equal to 25 °C and γ is −0.005°C^{-1}. T_{cell} is estimated as:

$$T_{cell} = k_1 + k_2 \bullet T_{air} + k_3 \bullet SWD + k_4 \bullet WS_{10} \tag{9}$$

where $k_1 = 4.3$ °C, $k_2 = 0.943$, $k_3 = 0.028$ °C m^2 W^{-1} and $k_4 = -1.528$ °C sm^{-1} [14]. T_{air}, WS_{10} and SWD are extracted from the WFD Dataset. If ambient conditions correspond to the standard test conditions, then F_{PV} is equal to 1.

To calculate the power capacity (P_{PV}), we first extract from the NASA Prediction of Worldwide Energy Resources [60] the daily average amount of the total solar radiation incident on a horizontal surface ($R_{d,m}$) (kWh m^{-2} day^{-1}) for the period 1983–2018. As the data is available for each month, it is aggregated on an annual basis:

$$P_{PV} = \left(\eta_{PV} \bullet A_{I-PV} \bullet \sum_{d,m} R_{d,m}\right) \Big/ (8760\ h/year) \tag{10}$$

The technical annual PV potential ($G_{PV,y}$) for each grid cell is calculated as:

$$G_{PV,y} = \eta_{PV} \bullet A_{I-PV} \bullet \sum_{d,m} R_{d,m} \tag{11}$$

where η_{PV} is the conversion efficiency, $A_{I\text{-}PV}$ is the area available for installing PV solar in each grid cell and the subscripts d, m, and y mean month, day and year, respectively. The area available for installing PV solar in each grid is calculated in the same manner as that for wind-power. In addition to the excluded areas described above, sites with an annual solar irradiance below 950 kWh/m^2 are excluded, as they appear uneconomical [46]. A conversion efficiency for PV utility-scale systems is assumed, as suggested in Ref. [47]:

$$\eta_{PV} = \eta_M \bullet \eta_{PR} \bullet \eta_{GC} \tag{12}$$

where η_M is the module efficiency (20%), η_{PR} is the performance ratio (75%), and η_{GC} is the share of land capturing energy (20%). Finally, for estimating the power capacity P_{PV} for each grid cell, the technical annual PV potential (GWh/year) is divided by 8760 h. The monthly PV power generation is calculated in the same manner.

2.3. Complementarity of wind, solar, and hydropower resources

As described above, we selected pairs of resources (hydro-solar, hydro-wind, solar-wind) at a country level with a Spearman correlation coefficient of at least −0.5 in monthly power generation. While there are numerous sites with significant wind- and solar-energy potential in the selected countries, not all of them offer a high complementarity with existing hydropower, and therefore are excluded from the analysis. The operation of hydropower aims at maximizing power generation over the long-term and is not intended to maximize complementarity to VRE resources. This certainly offers a further room for improvement. The capacity of wind, solar, and hydropower for these countries totals 24 GW, 102 GW, and 107 GW, respectively (see Fig. 3). The solar capacity is substantial, equaling about 95.3% of the existing hydropower capacity.

It is important to highlight that while this is a promising potential, it could be significantly limited by two factors. Firstly, some of these VRE resources are spatially heterogeneous, which might pose challenges for connection not only to the transmission and distribution networks but also to load centers. Secondly, even if the VRE are integrated into the system, the transmission system could offer only a limited capacity to incorporate these resources to balance the load in real time. Thus, a dedicated analysis is the transmission line is essential for performing definitive risk assessments.

For each of these resources, the average power generation throughout the entire twentieth century is estimated and then aggregated on a monthly basis at a country level. The average monthly power generation with a confidence level of 95% and broken down by ENSO phase, country, and resource is shown in Fig. 4. The figure shows that the uncertainty associated with regard to wind and solar power is significantly lower than that for hydropower. On the other hand, in all the selected countries the margin of error in neutral phases is significantly lower than that in nonneutral phases. This is caused not only by a larger spread in data for nonneutral ENSO phases, but also by the fact that there are fewer observations in 10th or 90th percentiles than between them.

To analyze the dependence between wind, solar, and hydropower, we performed a bivariate analysis, which is shown in Fig. 5. This graph shows the distributions of hydropower, wind and solar by country, highlighting the months of the year. In all countries, hydropower is negatively correlated to solar-power. Hydropower is also negatively correlated to wind power in Brazil and Mexico, but not in Argentina, where wind power is negatively correlated to solar but not simultaneously to hydropower. This topic requires further investigation. The influence of seasonal variability depends on the resource and the country. In Argentina, solar power generation is very clustered, and the distribution shows multiple peaks corresponding to the different months of the year. Solar resources in Argentina are located far away from the equator, where the solar radiation and day length strongly depend on the month of the year. A similar clustering is found in Brazil and Mexico, although less pronouncedly than in Argentina. In contrast, in countries near the equator (e.g., Colombia and Venezuela), solar-power is widespread and practically clustered in two groups, namely in dry and wet months. On the other hand, the influence of the month of the year on wind power is less evident than solar power in all countries.

2.4. Evaluation of different levels of penetration of VRE

2.4.1. Definition of portfolios – level of VRE penetration

In order to analyze the influence of different levels of penetration of VRE on the uncertainty in power generation, we created a set of portfolios. In these portfolios, the VRE capacity ranges between 0 and 100% of the maximal combined capacity of wind and solar power. Capacities for the different levels of penetration and their ratio relative to the hydropower capacities by country are shown in Fig. 6 and Table 1, respectively. Our measure for evaluating the risk of a power deficit is the 10th percentile of the driest months of the year for each country. The month with the lowest hydropower generation in the year is December in Argentina, September in Brazil, February in Colombia, April in

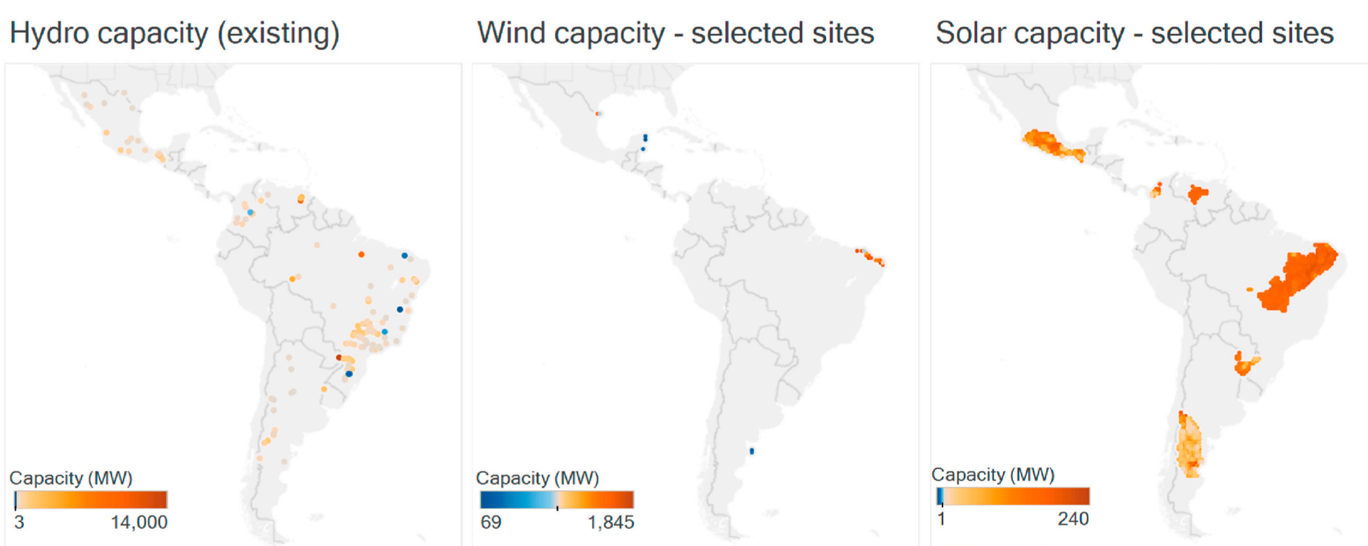

Type	Argentina	Brazil	Colombia	Mexico	Venezuela	Grand Total
Hydro	6,903	73,117	3,385	8,953	15,180	107,539
Solar	14,884	66,789	1,477	14,697	4,665	102,512
Wind	501	20,784		2,967		24,252
Grand Total	22,288	160,691	4,862	26,617	19,845	234,303

Fig. 3. Power capacity by resource for the selected sites (values in MW).

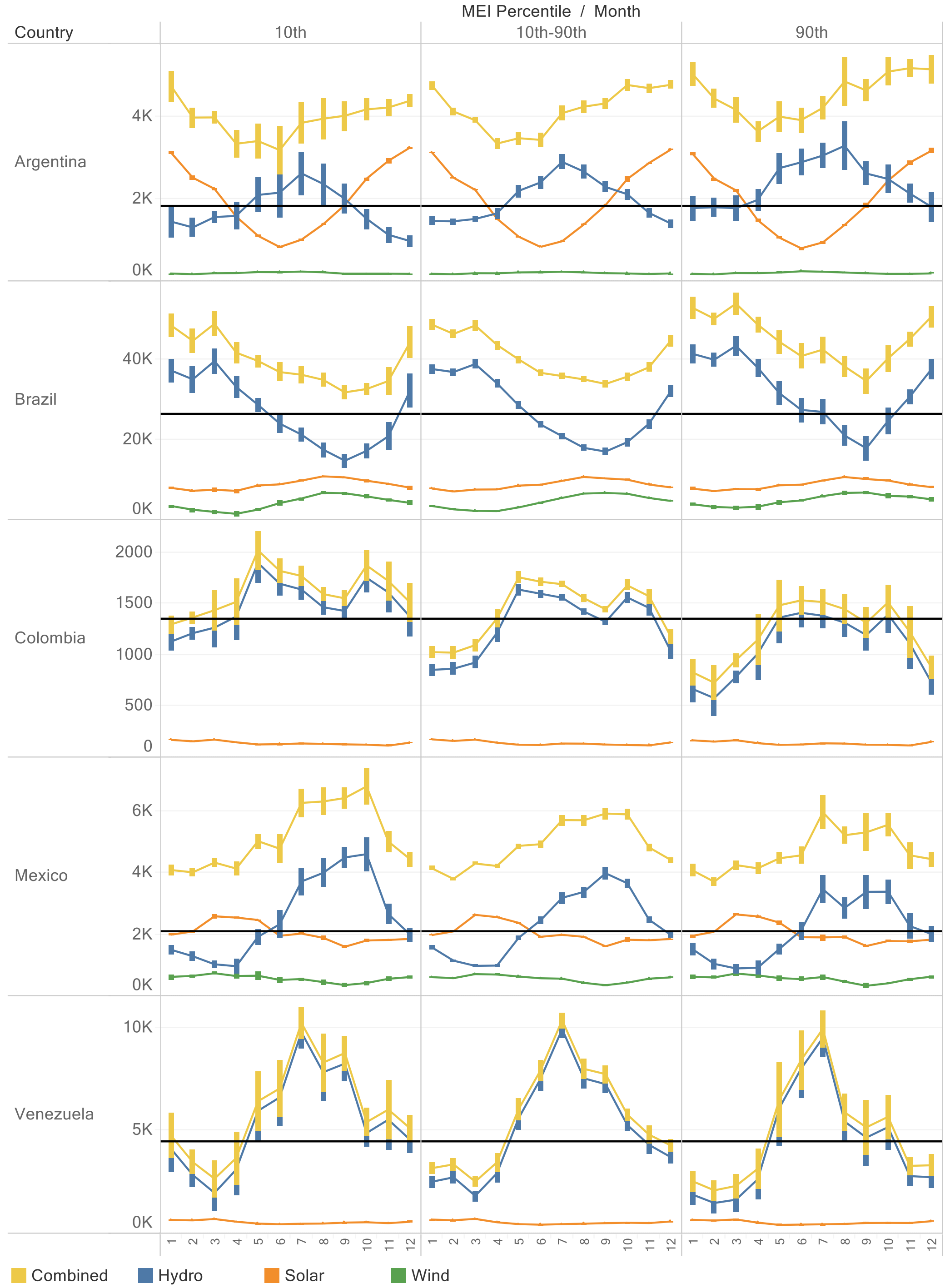

Fig. 4. Average monthly power generation in GWh broken down by ENSO phase, resource, and country. Color bars indicate a margin of error with a confidence level of 95%. Black lines represent the median of hydropower alone during neutral ENSO phases (10th-90th MEI percentile).

Mexico and March in Venezuela (see Fig. 4).

2.5. Probability density functions (PDFs)

Next, we calculated the probability density functions (PDFs) for the observed time series of average monthly power generation of wind, solar, and hydropower for these months throughout the entire twentieth century. The PDFs calculated for the driest month of the year in each country at different levels of VRE penetration are shown in Fig. 7.

By comparing the shape of the PDFs during the neutral ENSO phase in a hydro only system (i.e., 0% penetration by VRE), two groups can be identified. The PDFs for Venezuela and Colombia, i.e., the countries near the equator, show a large spread in values and multiple peaks with high rates of occurrence. In contrast, The PDFs for Argentina and Mexico present a somewhat smoother shape, with a quite pronounced peak, but with an occurrence rate of the peak comparable to that of Venezuela (in Argentina) and Colombia (in Mexico). Brazil's PDF exhibits a specific pattern that is similar to that of Argentina, but with a less pronounced

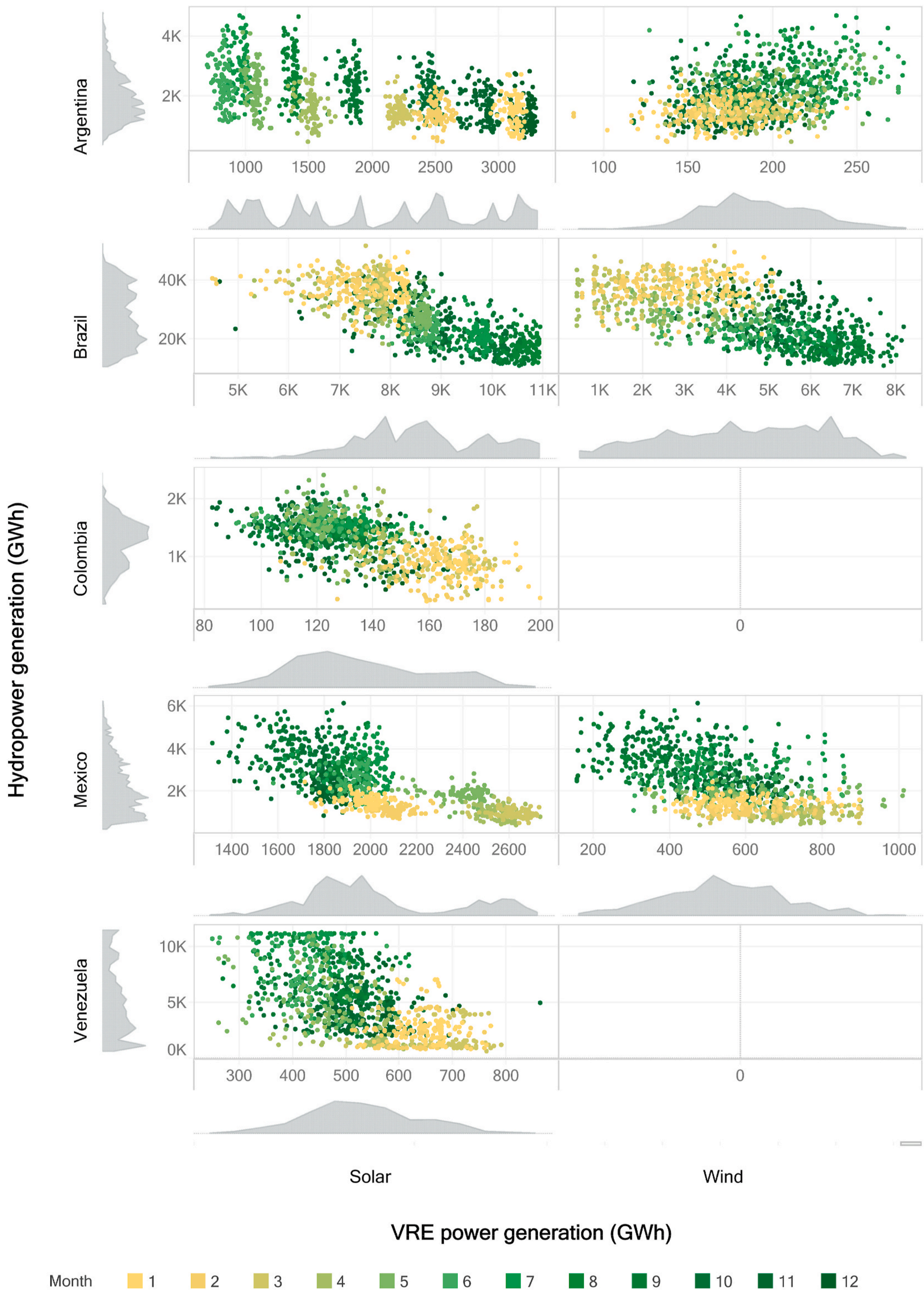

Fig. 5. Solar and wind power generation vs. hydropower generation by country in GWh. The colors indicate the month of the year.

peak.

For all countries, it is more likely that power generation during ENSO drought phases is—though with some exceptions—by far lower than during neutral phases, as can be expected. Results show that in all countries the monthly hydropower generation during ENSO drought phases could be between 5 and 50% lower than during neutral phases. The impact of ENSO droughts varies across countries. In Colombia and Argentina, for example, the reduction ranges between 25 and 50% depending on the percentile, while in Mexico, Brazil, and Venezuela it ranges between 5 and 30%. A higher penetration of VRE in the system increases the overall monthly power generation and affects the shape of the PDFs. However, the extent depends on the relevance of VRE in the national energy system. For example, the impact is quite low in Venezuela and Colombia, where the VRE capacity is rather small compared to their hydropower capacity (Fig. 6 and Table 1). Further general information on probability density functions and cumulative distribution functions is shown in Appendix C.

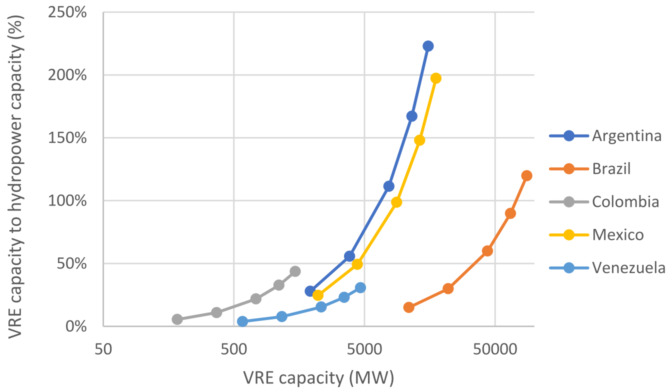

Fig. 6. VRE capacity (MW) vs. VRE to hydropower capacity, broken down by country.

2.6. Cumulative distribution functions (CDFs)

While these PDFs are the basis for a probabilistic assessment, it is difficult to observe differences and trends graphically. To improve the visualization of data, in addition to PDFs, we evaluated the associated cumulative distribution functions (CDFs) for the driest months by country. The CDFs calculated for the driest month of the year in each country at different levels of VRE penetration and ENSO phases are shown in Fig. 8. In addition, percentage differences between different levels of VRE penetration and hydropower alone are shown in Fig. 9 by ENSO phase and country.

Combining hydropower with VRE effectively increases the monthly power generation in the driest month of the year, both in drought and in neutral ENSO phases compared to hydropower alone. The increase differs between the countries and depends crucially on the corresponding VRE-hydropower capacity ratio. In Argentina and Mexico, the two countries with the largest VRE to hydropower capacity ratios (223% and 197%, respectively), combining hydropower with VRE could generate 400–600% more monthly power generation than hydropower alone. In Brazil, where the VRE capacity is 1.2 times as large as the hydropower capacity, this increase could go up to 150%. In Venezuela and Colombia, where the VRE-hydropower capacity ratio is 31 and 44%, respectively, the increase could go up to 60–70%.

For statistical reasons, the difference between a combined hydropower-VRE system and a hydropower alone system decreases with the percentile (i.e., cumulative probability). Thus, when hydropower is

Table 1
Aggregated VRE capacity (MW) and its relation to hydropower capacity.

Penetration (%)	VRE Capacity (MW)					VRE capacity to hydropower capacity (%)				
	Argentina	Brazil	Colombia	Mexico	Venezuela	Argentina	Brazil	Colombia	Mexico	Venezuela
12.5%	1923	10947	185	2208	583	28%	15%	5%	25%	4%
25%	3846	21893	369	4416	1166	56%	30%	11%	49%	8%
50%	7693	43787	739	8832	2333	111%	60%	22%	99%	15%
75%	11539	65680	1108	13248	3499	167%	90%	33%	148%	23%
100%	15385	87573	1477	17664	4665	223%	120%	44%	197%	31%

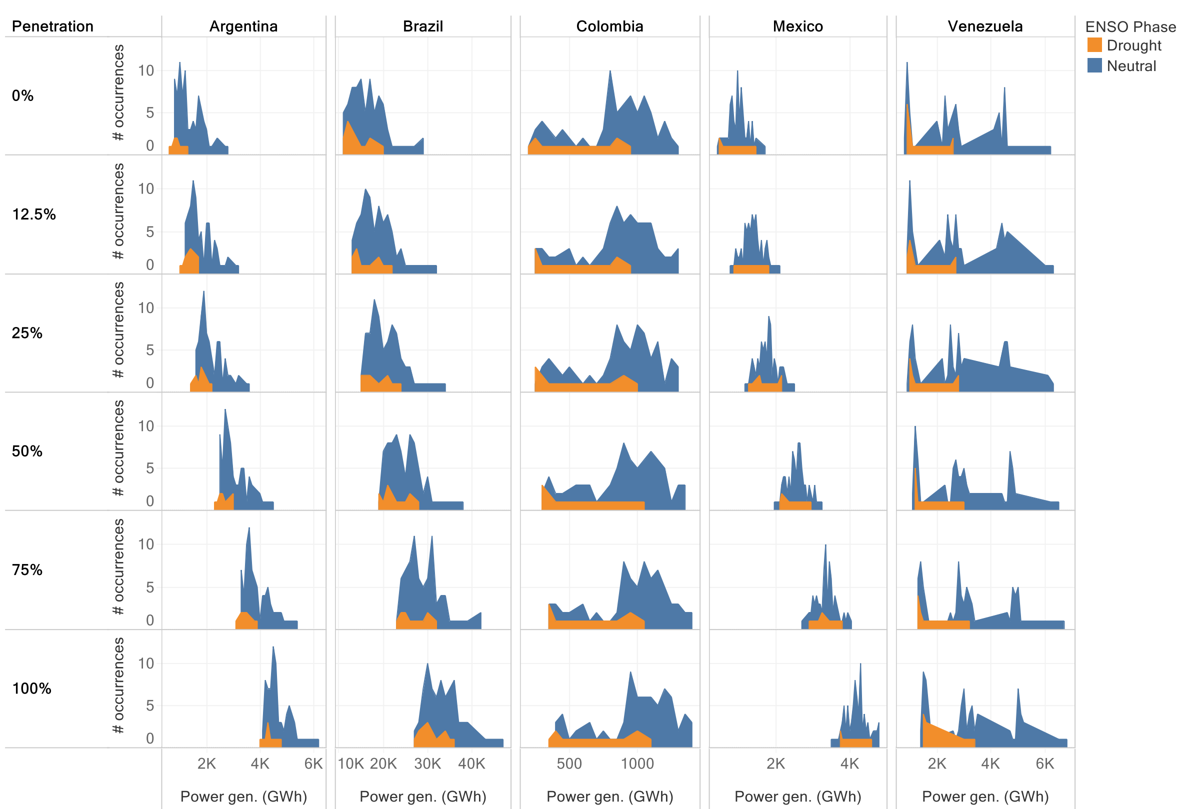

Fig. 7. Probability density functions (PDFs) for the monthly power generation (GWh/month) for the driest month of the year in each country at different levels of VRE penetration. The y-axis indicates the number of occurrences. The colors indicate the ENSO phase.

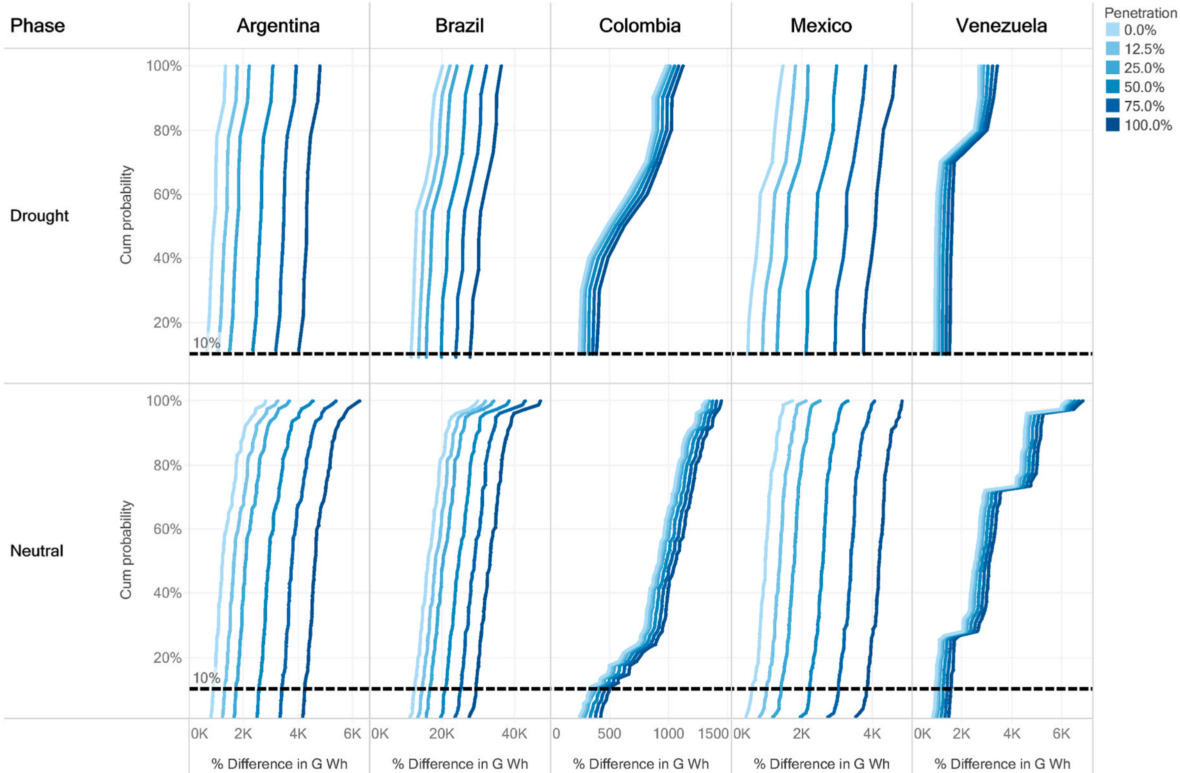

Fig. 8. Cumulative distribution functions (CDFs) for monthly power generation (GWh/month) for the driest months of the year at different levels of VRE penetration and ENSO phases by country. The colors indicate the level of VRE penetration. The dashed line represents the risk measure, i.e., the 10th percentile.

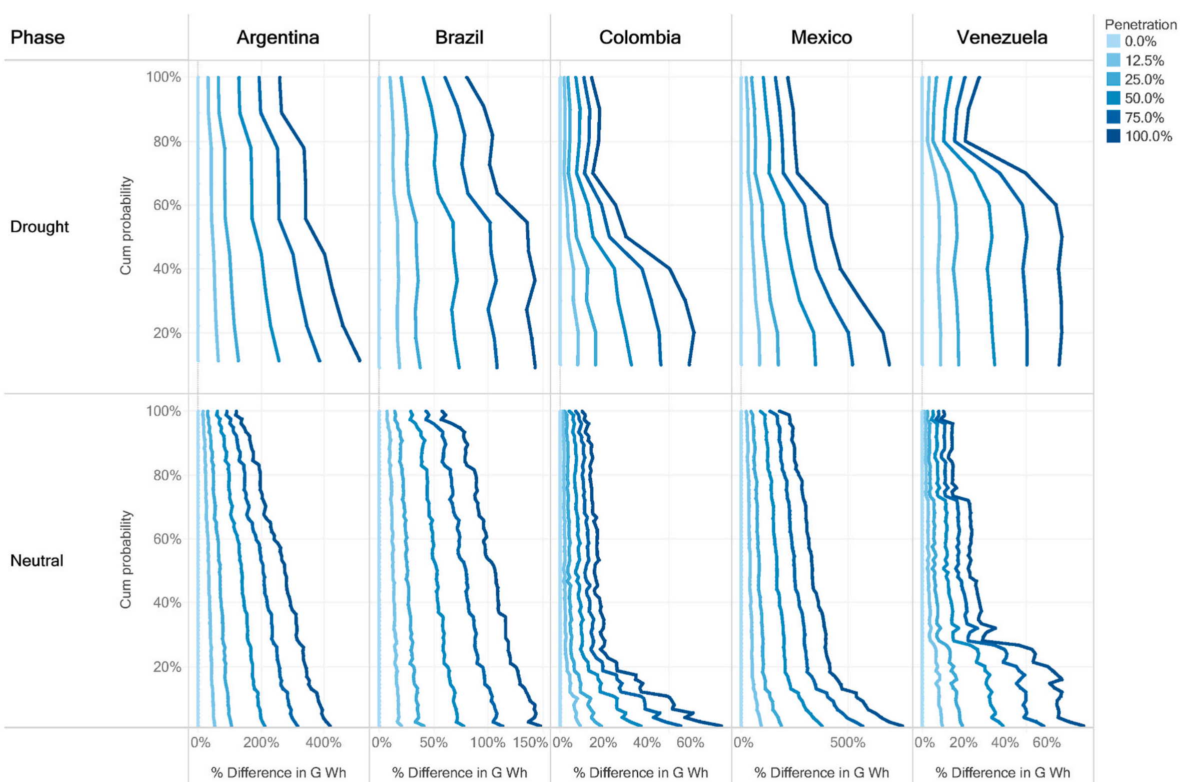

Fig. 9. Percentage difference in monthly power generation between the different levels of VRE penetration and hydropower alone for the driest month of the year. Data is disaggregated by ENSO phase and country.

combined with VRE, the increase in monthly power generation is more pronounced at low percentiles of cumulative probability. However, the pattern of the percentage difference differs between the countries and the ENSO phases. In Colombia and Venezuela, the two countries with the lowest VRE-hydropower capacity ratio, the impact of complementarity during neutral ENSO phases is highest at percentiles below 30%, independent of the market penetration of VRE. While the difference between a combined power system and a hydropower system alone drops in Colombia quite continuously from percentile 0–5% to percentile 30%, in Venezuela the differences at the lower end of the CDF are rather equal, and a noteworthy drop occurs only near 30%. In Colombia, the differences between a combined system and a hydropower system alone lessen quite continuously for percentiles higher than 30%, whereas in the case of Venezuela two steps can be identified, i.e., percentiles 75% and 95%; between these steps the differences between both systems are quite constant, independent of the market penetration rate.

The CDF profiles in the remaining countries exhibit similarities and differ from the profiles of Colombia and Venezuela. Common to the three remaining countries are the smoother differences between a combined system and hydropower alone compared to Colombia and Venezuela, especially during neutral ENSO phases. In the case of Argentina, differences between the systems drop continuously at higher percentiles, whereas in Mexico the differences between the systems decline rapidly at first (until percentile 10%) followed by a rather continuous drop. Brazil's pattern shows a continuous decline until percentile 90%, followed by a noteworthy drop. In the ENSO drought phase, the CDF patterns of all the countries are different. Differences between the systems also decline at higher percentiles for all market penetration rates, even though the declines are less pronounced in the ENSO drought phase than during neutral phases.

These patterns indicate that combining existing hydropower with complementary VRE effectively increase the probability of generating power, especially during droughts, either seasonal (i.e., lower percentiles) or caused by ENSO. The size and the pattern of the impacts differ between countries, which is partly noteworthy and needs to be the object of additional research.

2.7. Mitigation strategies

The strong impact of combining existing hydropower with complementary VRE, particularly at lower percentiles, is certainly advantageous as a strategy to mitigate a situation of a possible power deficit caused by seasonal variability or ENSO drought. Hence, we analyzed the 10th percentile of the cumulative distribution functions (dashed line in Fig. 8), which is our risk measure and represents the power deficit that occurs once every decade. Our primary interest is to understand how much wind and solar power are needed to counteract this power deficit, especially during ENSO drought phases. Thus, we extracted the power generation for the 10th percentile of the driest month for the different levels of VRE penetration by country (see Fig. 10). We identified two potential strategies, which are represented by a gray zone and described as follows:

- **First strategy (bottom threshold)**: a very moderate one, is to reach the level of power generation by hydropower alone during the driest month of the year in a neutral ENSO phase. This strategy represents the amount of VRE required to overcome the effect of the ENSO drought on hydropower alone.
- **Second strategy (top threshold)**: an ambitious one, is to reach the median annual value of hydropower alone in the neutral ENSO phase, which is represented with a black line in Fig. 4. Note that the median annual value is a significantly higher value than that during the driest month of the year. This second strategy represents the amount of VRE required not only to overcome the effect of the ENSO drought on hydropower, but also the effect of the seasonal drought.

The intersection between the orange line (representing the drought ENSO phases) and these two thresholds shows the VRE-hydropower capacity ratio required to overcome 1) the impact of drought ENSO phases and 2) seasonal droughts.

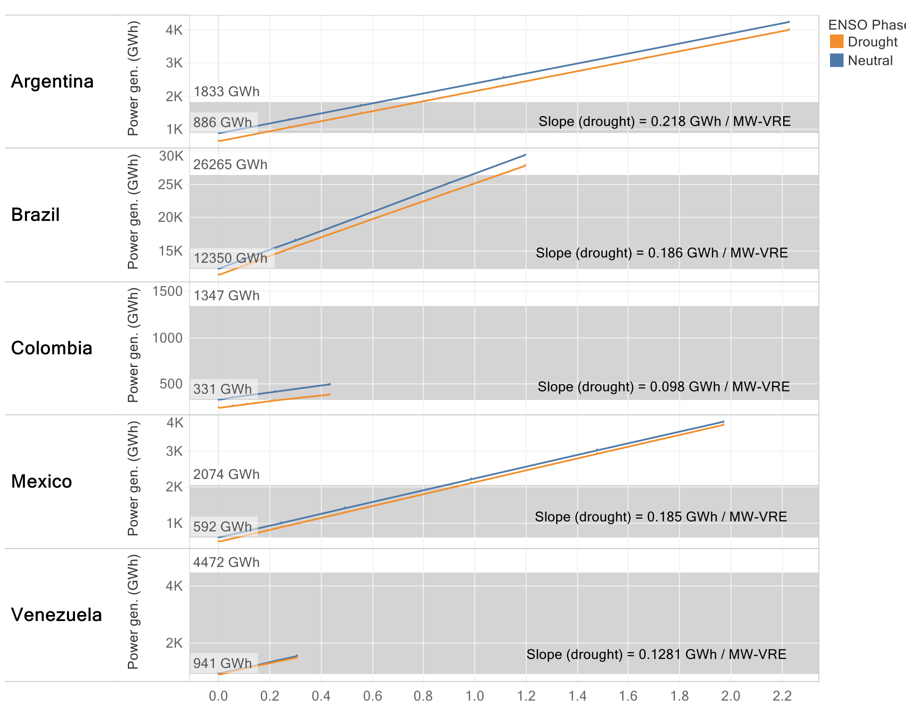

Fig. 10. Monthly power generation as a function of the VRE-hydropower capacity ratio for the 10th percentile of the driest month of the year, disaggregated by country. The bottom threshold represents the power generation for hydropower alone during neutral ENSO phases. The top threshold represents the median power generation for hydropower alone during neutral ENSO phases.

Our results show that to achieve the first strategy (i.e., 10th percentile of hydropower generation during neutral ENSO phases), a VRE-hydropower ratio between 0.05 and 0.22 is required. The largest value is required in Colombia (740 MW), the lowest in Venezuela (580 MW). To achieve the second strategy —i.e., reaching the median value for hydropower alone throughout the year in neutral ENSO phases—, it is necessary to maintain a significant VRE capacity. A VRE-hydropower capacity ratio of 0.8 would be required in Argentina (7 GW), while a ratio of 1 would be required in Mexico (8.8 GW) and 1.1 in Brazil (73 GW). In Colombia and Venezuela, the VRE capacity is insufficient to achieve this second strategy.

The slope of the line representing the 10th percentile of the driest month of the year during drought ENSO phases was also computed and is shown in Fig. 10. This slope embodies the effectiveness in the combination of resources to mitigate a potential power deficit. Results show that Argentina is the country with the most effective combination of resources to mitigate a power deficit, as each MW of installed VRE generates 0.218 GWh of additional power. It is followed by Brazil and Mexico, where each MW of installed VRE generates 0.185 GWh of power. In Venezuela and Colombia, the effectiveness is lowest, with 0.128 and 0.098 GWh/MW-VRE. A possible reason for this is that during the driest month of the year solar-power is less prevalent in countries located in the tropics of Cancer and Capricorn than in countries near the equator, which could result in a more effective combination of solar- and hydropower.

3. Conclusions

This paper quantifies the potential benefits of combining wind, solar, and hydropower to improve the reliability of renewable power generation from a probabilistic point of view. The analysis of the cumulative distribution functions (CDFs) of these resources for the entire twentieth century provides valuable insights.

Firstly, it shows that—depending on the country and the percentile—hydropower alone could be up to 50% lower during drought ENSO phases than during neutral phases. The countries most affected are Colombia and Venezuela, while the reduction is somewhat less severe in Argentina, Brazil, and Mexico.

Secondly, it shows that combining existing hydropower with complementary VRE offers the potential to reduce the risk of a power deficit during the 10th percentile of the driest months of the year, both in drought and neutral ENSO phases. Compared to hydropower alone, the combination of hydropower and VRE could increase the monthly power generation by 50–500%, depending on the country and level of VRE penetration. The potential increase is largest in Argentina and Mexico, where the maximal VRE-hydropower capacity ratio is highest (ranging between 2 and 2.2).

To enhance the reliability of power generation while lowering the carbon footprint, a promising strategy for the countries investigated in this study could be to increase their VRE capacities. The impact is in particular noteworthy during the most precarious periods of drought and dry seasons. However, the positive effect of complementarity differs in size and shape between the investigated countries. Although the general strategy could be same for all countries, the details should differ depending on the country. The country-specific strategies should take into account the proximity to the equator, which influences not only the size of the impacts of ENSO drought phases on hydropower production, but also on the optimal energy technology mix. For example, our results show that Argentina is the country with the most effective combination of resources to mitigate the power deficit, as each MW of installed VRE generates 0.218 GWh of additional power. It is followed by Brazil and Mexico with 0.185 GWh per MW of VRE and by Venezuela and Colombia with 0.128–0.098 GWh/MW-VRE, respectively. A possible reason for this trend is that during the driest months of the year solar power is less widespread in countries located in the tropics of Cancer and Capricorn than in countries near the equator, which could lead to a more effective combination of solar and hydropower.

While these results are promising, further research is required to validate them. For example, detailed techno-economic analyses of building complementary VRE power plants and expanding transmission lines is essential. Furthermore, an evaluation of socio-economic conditions, e.g., availability of financial resources or regulations in respect to investments and operation of VRE power plants, is necessary.

Author contributions

Miguel Gonzalez-Salazar: Conceptualization, Methodology, Data curation, Formal analysis, Investigation, Visualization, Writing – review & editing. Witold Roger Poganietz: Methodology, Formal analysis, Writing – review & editing, Supervision.

Declaration of competing interest

The authors declare that they have no known competing financial interests or personal relationships that could have appeared to influence the work reported in this paper.

Acknowledgements

This material has been produced under the Climate Compatible Growth programme, which is funded by UK aid from the UK government. However, the views expressed herein do not necessarily reflect the UK government's official policies. The authors received no external support for this work. The authors would like to thank the anonymous reviewer.

Nomenclature

A_{Add}	Area with additional environmental restrictions
A_I	Area available for installing renewables
$A_{I\text{-}PV}$	Area available for installing solar PV
$A_{I\text{-}W}$	Area available for installing wind turbines in each grid cell
A_{LC}	Total land cover area
A_{PL}	Protected land
A_S	Area suitable for installing renewables
A_{UL}	Unsuitable land for installing renewables
A_{TU}	Area technically uneconomical for installing renewables
cov	Covariance
ENSO	El Niño-Southern Oscillation
F_{PV}	Performance factor for solar photovoltaic cells
G_{PV}	Technical annual solar PV potential

G_W	Technical annual wind potential
k	Constant
MEI	Multivariate ENSO Index
MODIS	Moderate Resolution Imaging Spectroradiometer
N_W	Occupation area per wind turbine
P	Power capacity
P_{Surf}	Surface pressure
$P_{PV,\ W}$	Power capacity of solar photovoltaic cells and wind turbines
PG	Annual power generation
PG_W	Annual power generated by an individual wind turbine
PV	Solar photovoltaic cells
r.x	Ranking variable
R	Gas constant
R_d	Total solar radiation incident on a horizontal surface
$S_{x\leftrightarrow y}$	Spearman correlation coefficient
SWD	Downward shortwave radiation flux
SWD_{TC}	SWD at test conditions
T_{air}	Air temperature
T_{cell}	PV cell temperature
T_{TC}	PV cell temperature at standard conditions
WFD	WATCH forcing data
WS	Wind speed
σ	Standard deviation
ρ	Air density
η_{GC}	Share of land capturing energy
η_{GT}	Gas turbine efficiency
η_M	Module efficiency
η_{PV}	PV solar conversion efficiency
η_{PR}	Performance ratio

Appendix A. Additional details on literature review

Study	Resources	Geographic scale	Analysis of ENSO	Approach
Gunturu & Hallgren [5]	Hydro, wind	National	Yes	Deterministic
Viviescas et al. [16]	Hydro, PV, wind	Multi-national	Yes	Deterministic
Henao et al. [18]	Hydro, PV, wind	National	Yes	Deterministic
Vergara et al. [19]	Hydro, wind	National	No	Deterministic
Paredes & Ramirez [20]	Hydro, PV, wind	National	No	Deterministic
Rosa et al. [21]	Hydro, PV, wind	Sub-national	No	Deterministic
Pianezzola et al. [22]	Solar, wind	National	No	Deterministic
Chaer et al. [23]	Hydro, PV, wind	National	No	Deterministic
Beluco et al. [24]	Hydro, PV	National	No	Deterministic
Silva et al. [25]	Hydro, wind (offshore)	National	No	Deterministic
Ávila et al. [26]	Hydro, wind	National	No	Stochastic
Neto et al. [27]	Solar, wind, tidal	National	No	Deterministic
Cantao et al. [28]	Hydro, wind	National	No	Deterministic
BID [29]	Hydro, PV, wind	Multi-national	Yes	Deterministic
Gonzalez-Salazar & Poganietz [30]	Hydro, PV, wind	Multi-national	Yes	Deterministic
Li et al. [31]	Hydro, PV	National	No	Stochastic
Ming et al. [32]	Hydro, PV	National	No	Stochastic
Huang et al. [33]	Hydro, PV, wind	National	No	Stochastic
Zhang et al. [34]	Hydro, wind	National	No	Stochastic
Schmidt et al. [35]	Hydro, PV, wind	National	No	Stochastic
Luz & Moura [36]	Hydro, PV, wind	National	No	Deterministic
Xu et al. [37]	Hydro, wind	National	No	Stochastic
Denault et al. [38]	Hydro, wind	National	No	Stochastic

Appendix B. Additional technical information

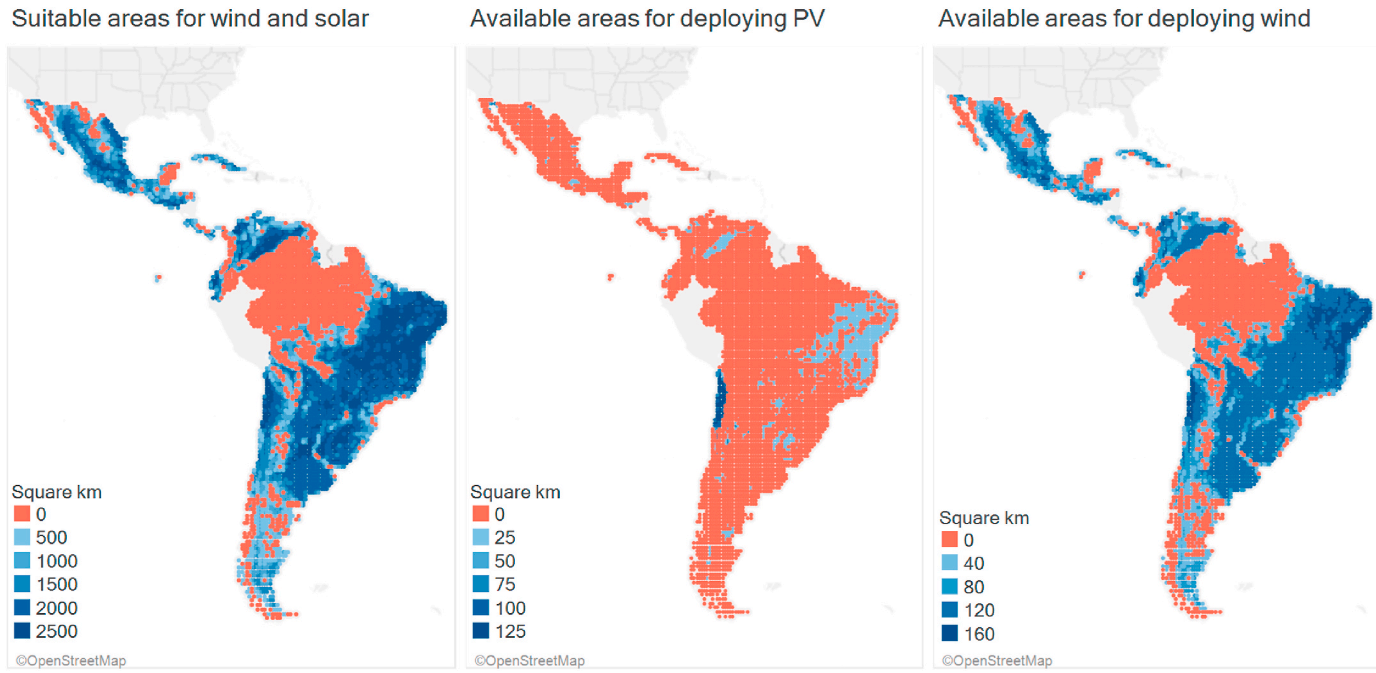

Fig. 11. (Left) Suitable areas for deploying solar PV and wind after excluding forests, environmentally sensitive areas, and water bodies. (Middle) Available areas for deploying solar PV after applying availability factors based on land cover. (Right) Available areas for deploying wind-power after applying availability factors based on land cover. Countries with no data available are shown in gray. Values are shown per cell of 0.5 x 0.5°.

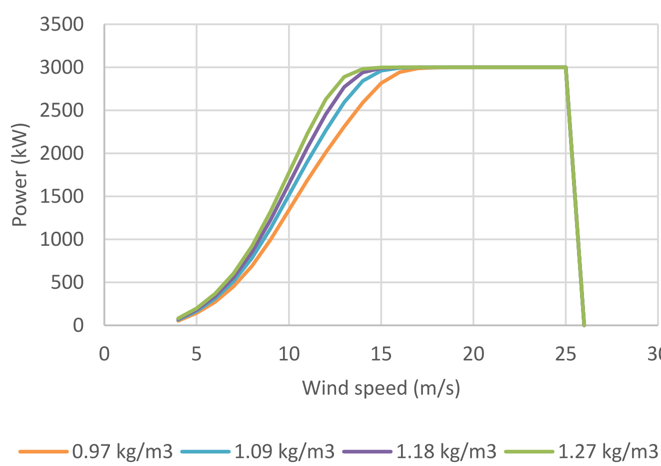

Fig. 12. Power curve for the Vestas V90–3.0 MW.

Appendix C. Probability density functions (PDFs) and cumulative density functions (CDFs)

PDFs and CDFs provide critical information for a risk assessment. PDFs reveal the distribution of the probability of occurrence of production levels within a given range, in our case between zero and maximum generation of power (a function of the power capacity). CDFs represent the cumulative probability of a variable x, which is the probability that the variable x takes on a value less or equal to x. The concept is better explained through an example. Fig. 13 shows two exemplary cumulative distribution functions, namely y_1 and y_2, which are functions of a variable x. Assuming, for example, that x is equal to 2, there is a 90% probability that y_2 is lower or equal than 2, while it is only 56% for y_1. Conversely, it also means that for a given percentile, like 56% (i.e., 56% probability), y_1 is likely to have a higher value (2) than y_2 (1.2). The slope of the curves indicates how spread out the values are. A slope that is steep indicates that values are similar and not spread. On the contrary, a flattened slope indicates that data is spread [61]. In this example both curves flattened at the end; this indicates that these are possible outliers. Hence, observations on the upper bound of the variable x result in small increases in the cumulative probability. In our example, there is 95% probability that x is lower than 3.7 for y_1 and lower than 2.5 for y_2. In many applications CDFs are preferred over PDFs because their indication of the probability of a random variable is intuitive and can be seen graphically, while in PDFs they require the calculation of the area under the curve for a given interval [62].

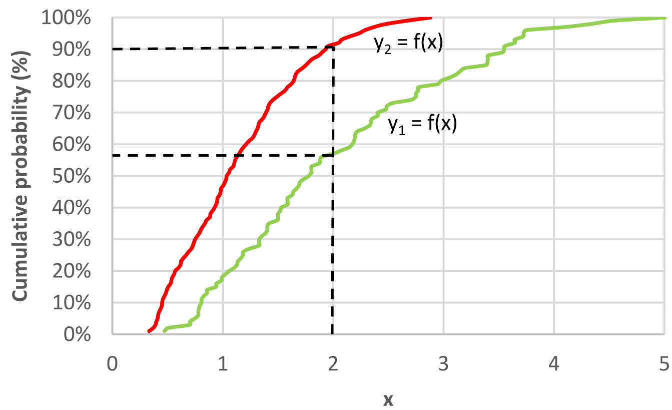

Fig. 13. Example of two cumulative distribution functions (CDFs).

References

[1] P. Ward, B. Jongmann, M. Kummu, M. Dettinger, F. Sperna Weiland, H. Winsemius, Strong influence of El Niño Southern Oscillation on flood risk around the world, Proc. Natl. Acad. Sci. U.S.A. 111 (44) (2014) 15659–15664.

[2] J. Ng, S. Turner, S. Galelli, Influence of El Niño southern oscillation on global hydropower production, Environ. Res. Lett. 12 (2017), 034010.

[3] P. Cashin, K. Mohaddes, M. Raissi, Fair weather or foul? The macroeconomic effects of El Niño, J. Int. Econ. (2017) 37–54.

[4] IPCC, Summary for Policymakers. Climate Change 2013: the Physical Science Basis. Contribution of Working Group I to the Fifth Assessment Report of the Intergovernmental Panel on Climate Change, Cambridge Univ Press, Cambridge, UK, 2013.

[5] U. Gunturu, W. Hallgren, Asynchrony of wind and hydropower resources in Australia, Sci. Rep. 7 (2017) 8818.

[6] N. Voisin, A. Hamlet, L. Graham, D. Pierce, T. Barnett, D. Lettenmaier, The role of climate forecasts in western U.S. Power planning, J. Appl. Meteorol. Climatol. 45 (2006) 653–673.

[7] D. Watts, P. Durán, Y. Flores, How does El Niño Southern Oscillation impact the wind resource in Chile? A techno-economical assessment of the influence of El Niño and La Niña on the wind power, Renew. Energy 103 (2017) 128–142.

[8] IRENA, Renewable Energy Market Analysis. Latin America, International Renewable Energy Agency, Abu Dhabi, 2016.

[9] E. Moran, M. Lopez, N. Moore, N. Müller, D. Hyndman, Sustainable hydropower in the 21st century, Proc. Natl. Acad. Sci. USA 115 (47) (2018) 11891–11898.

[10] S. Arango, E. Larsen, The environmental paradox in generation: how South America is gradually becoming more dependent on thermal generation, Renew. Sustain. Energy Rev. 14 (2010) 2956–2965.

[11] J. do Prado, J. Logan, F. Flores-Espino, Options for Resilient and Flexible Power Systems in Select South American Economies, Joint Institute for Strategic Energy Analysis, National Renewable Energy Laboratory (NREL), Golden, 2019.

[12] IRENA, Global Energy Transformation: A Roadmap to 2050, International Renewable Energy Agency, Abu Dhabi, 2018.

[13] E. Bianchi, A. Solarte, T. Guozden, Large scale climate drivers for wind resource in Southern South America, Renew. Energy 114 (2017) 708–715.

[14] S. Jerez, et al., The impact of climate change on photovoltaic power generation in Europe, Nat. Commun. 6 (2015).

[15] Edenhofer, et al., IPCC special report on renewable energy sources and climate change mitigation, in: Prepared by Working Group III of the Intergovernmental Panel on Climate Change, Cambridge University Press, Cambridge and New York, 2011.

[16] Viviescas, et al., Contribution of variable renewable energy to increase energy security in Latin America: complementarity and climate change impacts on wind and solar resources, Renew. Sustain. Energy Rev. 113 (2019) 13.

[17] J. Jurasz, F. Canales, A. Kies, M. Guezgouz, A. Beluco, A review on the complementarity of renewable energy sources: concept, metrics, application and future research directions, Sol. Energy 195 (2019) 703–724.

[18] F. Henao, J. Viteri, Y. Rodríguez, J. Gómez, I. Dyner, Annual and interannual complementarities of renewable energy sources in Colombia, Renew. Sustain. Energy Rev. 134 (2020).

[19] W. Vergara, A. Deeb, N. Toba, P. Cramton, I. Leino, Wind Energy in Colombia. A Framework for Market Entry, The World Bank, Washington, 2010.

[20] J. Paredes, J. Ramírez, Variable Renewable Energies and Their Contribution to Energy Security: Complementarity in Colombia, Inter-American Development Bank, Washington, 2017.

[21] C. Rosa, K. Costa, E. Christo, P. Bertahone, Complementarity of hydro, photovoltaic, and wind power in rio de Janeiro state, Sustainability 9 (1130) (2017).

[22] G. Pianezzola, A. Krenzinger, F. Canales, Complementarity maps of wind and solar energy resources fo rio grande do sul, Brazil, Energy Power Eng. 9 (2017) 489–504.

[23] R. Chaer, M. Gurin, E. Cornalino, M. Draper, R. Terra, G. Abal, R. Alonso, Complementariedad de las Energías Renovables en Uruguay y valorización de proyectos para el filtrado de su variabilidad, Fundación Julio Ricaldoni, Montevideo, 2014.

[24] A. Beluco, P. Souza, A. Krenzinger, A dimensionless index evaluating the time complementarity between solar and hydraulic energies, Renew. Energy 33 (2008) 2157–2165.

[25] A. Silva, F. Pimenta, A. Assireu, M. Spyrides, Complementarity of Brazil's hydro and offshore wind power, Renew. Sustain. Energy Rev. 56 (2016) 413–427.

[26] L. Ávila, M. Mine, E. Kaviski, D. Detzel, Evaluation of hydro-wind complementarity in the medium-term planning of electrical power systems by joint simulation of periodic streamflow and wind speed time series: a Brazilian case study, Renew. Energy 167 (2021) 685–699.

[27] P. Neto, O. Saavedra, D. Oliveira, The effect of complementarity between solar, wind and tidal energy in isolated hybrid microgrids, Renew. Energy 147 (2020) 339–355.

[28] M. Cantao, M. Bessa, R. Bettega, D. Detzel, J. Lima, Evaluation of hydro-wind complementarity in the Brazilian territory by means of correlation maps, Renew. Energy 101 (2017) 1215–1225.

[29] BID, La red del futuro. Desarrollo de una red eléctrica limpia y sostenible para América Latina, Banco Interamericano de Desarrollo, Washington, 2017.

[30] M. Gonzalez-Salazar, W. Poganietz, Evaluating the complementarity of solar, wind and hydropower to mitigate the impact of El Niño Southern Oscillation in Latin America, Renew. Energy 174 (2021) 453–467.

[31] H. Li, P. Liu, S. Guo, B. Ming, L. Cheng, Z. Yang, Long-term complementary operation of a large-scale hydro-photovoltaic hybrid power plant using explicit stochastic optimization, Appl. Energy 238 (2019) 863–875.

[32] B. Ming, P. Liu and L. Cheng, "An integrated framework for optimizing large hydro–photovoltaic hybrid energy systems: capacity planning and operations management," J. Clean. Prod., vol. 306, 2021.

[33] K. Huang, P. Liu, B. Ming, J. Kim, Y. Gong, Economic operation of a wind-solar-hydro complementary system considering risks of output shortage, power curtailment and spilled water, Appl. Energy 290 (2021).

[34] Y. Zhang, C. Cheng, R. Cao, G. Li, J. Shen and X. Wu, "Multivariate probabilistic forecasting and its performance's impacts on long-term dispatch of hydro-wind hybrid systems," Appl. Energy, vol. 283, 2021.

[35] J. Schmidt, R. Cancella, A. Pereira, An optimal mix of solar PV, wind and hydro power for a low-carbon electricity supply in Brazil, Renew. Energy 85 (2016) 137–147.

[36] T. Luz, P. Moura, 100% Renewable energy planning with complementarity and flexibility based on a multi-objective assessment, Appl. Energy 225 (2019).

[37] B. Xu, F. Zhu, P. Zhong, J. Chen, W. Liu, Y. Ma, L. Guo, X. Deng, Identifying long-term effects of using hydropower to complement wind power uncertainty through stochastic programming, Appl. Energy 253 (2019).

[38] M. Denault, D. Dupuis, S. Couture-Cardinal, Complementarity of hydro and wind power: improving the risk profile of energy inflows, Energy Pol. 37 (12) (2009) 5376–5384.

[39] W. Zappa, M. van den Broek, Analysing the potential of integrating wind and solar power in Europe using spatial optimisation under various scenarios, Renew. Sustain. Energy Rev. 94 (2018) 1192–1216.

[40] K. Engeland, M. Borga, J. Creutin, B. Francois, M. Ramos, J. Vidal, Space-time variability of climate variables and intermittent renewable electricity production - a review, Renew. Sustain. Energy Rev. 79 (2017) 600–617.

[41] K. Wolter, M. Timlin, El Niño/Southern Oscillation behaviour since 1871 as diagnosed in an extended multivariate ENSO index (MEI.ext), Int. J. Climatol. 31 (2011) 1074–1087.

[42] M. Friedl, D. Sulla-Menashe, MCD12C1 MODIS/Terra+Aqua Land Cover Type Yearly L3 Global 0.05Deg CMG V006 [Data Set], NASA EOSDIS Land Processes DAAC, 2018, https://doi.org/10.5067/MODIS/MCD12C1.006 [Online]. Available: [Accessed 1 11 2018].

[43] European Union, Digital Observatory for Protected Areas, European Union, 2017 [Online]. Available: https://dopa.jrc.ec.europa.eu [Accessed 1 2 2019].
[44] S. Saura, L. Bastin, L. Battistella, A. Mandrici, G. Dubois, Protected areas in the world's ecoregions: how well connected are they? Ecol. Indicat. 76 (2017) 144–158.
[45] X. Lu, M. McElroy, J. Kiviluoma, Global potential for wind-generated electricity, Proc. Natl. Acad. Sci. USA 106 (27) (2009) 10933–10938.
[46] A. Korfiati, C. Gkonos, F. Veronesi, A. Gaki, S. Grassi, R. Schenkel, S. Volkwein, M. Raubal, L. Hurni, Estimation of the global solar energy potential and photovoltaic cost with the use of open data, Int. J. Sustain. Energy Plann. Manag. 9 (2016) 17–30.
[47] Y. Deng, M. Haigh, W. Pouwels, L. Ramaekers, R. Brandsma, S. Schimschar, J. Grözinger, D. de Jager, Quantifying a realistic, worldwide wind and solar electricity supply, Global Environ. Change 31 (2015) 239–252.
[48] S. Turner, J. Ng, S. Galelli, Examining global electricity supply vulnerability to climate change using a high-fidelity hydropower dam model, Sci. Total Environ. 590–591 (2017) 663–675.
[49] Lehner, et al., High-resolution mapping of the world's reservoirs and dams for sustainable river-flow management, Front. Ecol. Environ. 9 (9) (2011).
[50] ICOLD, World Register of Dams Version Updates 1998-2009, International Commission on Large Dams, Paris, France, 2011. www.icold-cigb.net.
[51] Global Energy Observatory, Information on Global Energy Systems and Infrastructure, Global Energy Observatory, 2016 [Online]. Available: http://globalenergyobservatory.org. (Accessed 1 September 2019). Accessed.
[52] G. Weedon, S. Gomes, P. Viterbo, W. Shuttleworth, E. Blyth, H. Österle, J. Adam, N. Bellouin, O. Boucher, M. Best, Creation of the WATCH Forcing Data and its use to assess global and regional reference crop evaporation over land during the twentieth century, J. Hydrometeorol. 12 (5) (2011) 823–848, https://doi.org/10.1175/2011JHM1369.1.
[53] J. Alcamo, P. Döll, T. Henrichs, F. Kaspar, B. Lehner, T. Rösch, S. Siebert, Development and testing of the WaterGAP 2 global model of water use and availability, Hydrol. Sci. J. 48 (3) (2003) 317–337.
[54] P. Döll, B. Lehner, Validation of a new global 30-min drainage direction map, J. Hydrol. 258 (1–4) (2002) 214–231.
[55] S. Turner, S. Galelli, Water Supply Sensitivity to Climate Change: an R Package for Implementing Reservoir Storage Analysis in Global and Regional Impact Studies, vol. 76, Environmental Modelling & Software, 2016, pp. 13–19.
[56] IRENA, Future of Wind: Deployment, Investment, Technology, Grid Integration and Socio-Economic Aspects (A Global Energy Transformation Paper), International Renewable Energy Agency, Abu Dhabi, 2019.
[57] CEH, Water and global change (WATCH) forcing data (WFD) - 20th century, Centre for Ecology & Hydrology (CEH), Natural Environment Research Council, [Online]. Available: https://catalogue.ceh.ac.uk [Accessed 9 9 2019].
[58] Vestas, General Specification V90 - 3.0 MW, Vestas Wind Systems, Ringkoebing, 2004.
[59] A. Troccoli, et al., Creating a proof-of-concept climate service to assess future renewable energy mixes in Europe: an overview of the C3S project, Adv. Sci. Res. 15 (2018) 191–205.
[60] NASA, Prediction of worldwide energy resources (POWER), National Aeronautics and Space Administration (NASA), [Online]. Available: https://power.larc.nasa.gov/ [Accessed 1 1 2019].
[61] Lazymodellingcrew, Lazymodellingcrew, 21 August 2020 [Online]. Available: https://lazymodellingcrew.com/post/post_14_reading_like_a_fourthgrader_ta/ [Accessed 2022 August 25].
[62] P. Bruce, A. Bruce, Practical Statistics for Data Scientists, O'Reilly Media, Inc., 2017.